Super-Resolution from Image Sequence under Influence of Hot-Air Optical Turbulence

Masao Shimizu, Shin Yoshimura, Masayuki Tanaka, and Masatoshi Okutomi
Tokyo Institute of Technology, Japan

Abstract

The appearance of a distant object, when viewed through a telephoto-lens, is often deformed nonuniformly by the influence of hot-air optical turbulence. The deformation is unsteady: an image sequence can include nonuniform movement of the object even if a stationary camera is used for a static object. This study proposes a multi-frame super-resolution reconstruction from such an image sequence. The process consists of the following three stages. In the first stage, an image frame without deformation is estimated from the sequence. However, there is little detailed information about the object. In the second stage, each frame in the sequence is aligned non-rigidly to the estimated image using a non-rigid deformation model. A stable non-rigid registration technique with a B-spline function is also proposed in this study for dealing with a textureless region. In the third stage, a multi-frame super-resolution reconstruction using the non-rigid deformation recovers the detailed information in the frame obtained in the first stage. Experiments using synthetic images demonstrate the accuracy and stability of the proposed non-rigid registration technique. Furthermore, experiments using real sequences underscore the effectiveness of the proposed process.

1. Introduction

The refraction index of air depends on the ambient air pressure, temperature, humidity, carbon dioxide level, and air dust density. Moreover, the condition of air in the atmosphere is not homogeneous. An increase in temperature at a land surface which receives direct sunlight causes a nonuniform temperature distribution above the surface. The temperature distribution then generates air convection, which makes the distribution unsteady.

Refraction of light occurs on a border of two materials. Light travels on a curved line in a medium-like air, which changes its relative refraction index nonuniformly and continuously. The atmosphere moves by convection or wind, which changes the curved line along with the movement of the air. The hot-air optical turbulence, a so-called *heat devil*, is derived from such air nonuniformity and movement. A static object is deformed in an observed image by the optical turbulence, even if it is taken by a stationary camera. Moreover, the deformation is not constant for the image position and time; the real appearance of the object will never be observed.

Figure 1 shows example images taken under the influence of optical turbulence [1] . The images are close-up images of a sequence in 0.2 seconds interval for a far distant object taken through a telephoto-lens. Every image includes nonuniform deformations, which vary by time.

The real appearance of the object must be estimated from such observations. However, from another perspective, the movement can be considered as an observation of the slightly different position of the object. This allows enhancement of the image resolution using multi-frame super-resolution reconstruction, even if a stationary camera is used for a static object. The reconstruction process requires an accurate and stable non-rigid image registration technique.

Non-rigid image registration has been studied widely in medical-image processing [2],[5],[6] to align images taken at different times. In the non-rigid deformation model, the image to be aligned is deformed by changing the positions of the control points placed on the image. A positional interpolation for the deformed image requires a basis function for obtaining smoothly changing positions between the control points. The thin-plate spline (TPS) function [2] and the B-spline function [7] have been used for the basis function. The number of deformation parameters for these basis functions depends on the degree of deformation to align the image.

The deformation model with the TPS basis function

[1] Image degradations by a "bad" weather condition are comprehensively studied in [11]. Our approach utilizes another aspect of meteoric phenomena.

978-1-4244-2243-2/08/$25.00 ©2008 IEEE

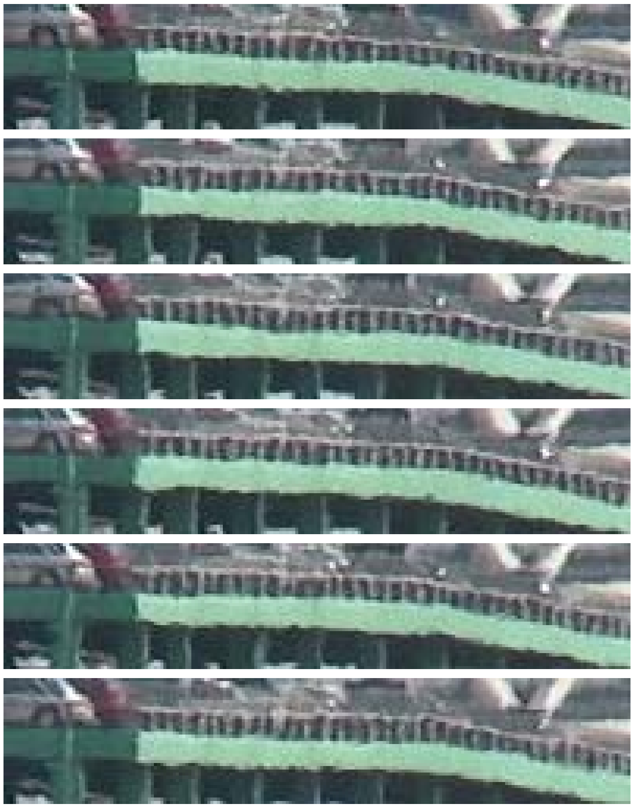

Figure 1. Several frames from a sequence for a far distant object taken through a telephoto lens.

has no restriction of the control point placement. The model also has a characteristic by which the displacement of a deformation at an interest point in an image tracks perfectly to the control point position. These characteristics enable the TPS basis function to be used in a feature-based non-rigid registration. However, it is generally difficult to obtain a sufficient number of corresponding feature points with satisfactory accuracy to align images in sub-pixel accuracy. For this issue, a method to improve the registration accuracy has been proposed using correspondence between curves [1]. A parameter estimation method for the TPS basis function by an area-based registration has also been proposed [8].

On the other hand, the non-rigid deformation model with the B-spline basis function [12] has less computational cost in transforming the image position than the other basis functions. This advantage enables the use of an area-based registration technique [5],[6] to align images with sub-pixel accuracy. However, the existing estimation methods of numerous parameters for the non-rigid deformation model become unsteady for a textureless or noisy region. In relation to this issue, a method to increase the parameter numbers by estimating the deformation [13] and a method to learn the basis of the non-rigid deformation [9] have been proposed.

This study proposes a multi-frame super-resolution reconstruction from an image sequence under influence of optical turbulence. This paper is organized as follows. Section 2 describes a method to estimate an image without deformation after investigating the characteristics of the nonuniform movement in the sequence under influence of optical turbulence. Section 3 proposes a stable non-rigid registration technique with the B-spline function, after representing the B-spline non-rigid motion model. A multi-frame super-resolution using the non-rigid model to estimate the detailed information is also described. Section 4 presents experiments using synthetic images to investigate the accuracy and stability of the proposed non-rigid registration technique. Experiments using real sequences are also presented. This paper concludes with remarks in Section 5.

2. Object Appearance Estimation

2.1. Characteristics of the Deformation Movement

Image deformation in the observed frame arises from a global motion and a local motion. The global motion is caused by the camera movement or object motion; it is representable by a translational or affine motion model. The local motion is a residual motion after compensating the global motion of the frame. It is representable by a non-rigid motion model.

A sequence taken using a hand-held camera includes global motion in many cases. Some sequences taken using a stationary camera with a telephoto lens also include global motion resulting from wind or earth tremors. The global motion can be removed from the sequence by compensating the estimated global motion for each frame to a reference frame. The global motion is obtainable using a common registration technique with a translational or affine motion model for a sufficiently large region of interest in the frame. The estimated global motion here includes an error because the two frames are not perfectly identical; both frames involve different deformation according to the local motion.

Figure 2 depicts the local translational motion, which is the tracking result for the rear tire of the silver car in Fig. 1, throughout the 900 frames in the sequence, after the global motion compensation. The figure also portrays a histogram of the horizontal and vertical components of the motion, with their Gaussian fitted curves. The histogram of the local motion can be approximated as a two-dimensional zero-mean Gaussian.

The local motion is a symmetrical distribution cen-

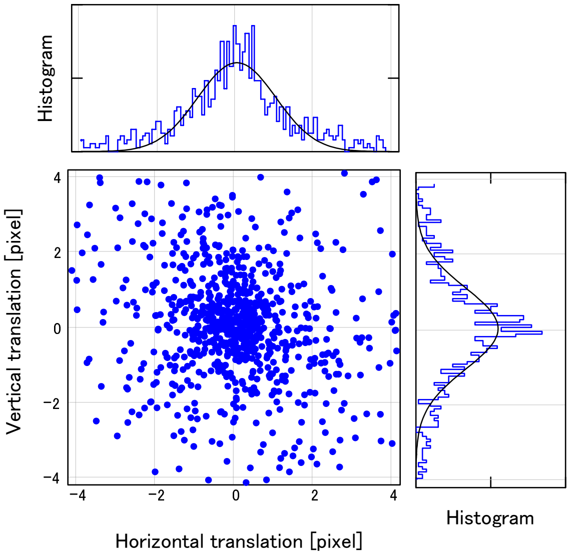

Figure 2. Deformation movement after removing the global motion.

tered at a position without any motion if the observation is a sufficiently long period. The standard deviation of the distribution can be estimated from the sequence. It depends on the lens focal length, the image size in pixels, the object distance, and the characteristics of the medium between the lens and the object.

2.2. Averaging the Frames

The object appearance without the local motion can be estimated by simply averaging the observed frames in the image sequence.

The averaging operation of the frames without global motion is equivalent to the Gaussian convolution of the real object appearance without any motion if the local motion is a normal distribution with mean zero and standard deviation σ:

$$\frac{1}{N}\sum_{k=1}^{N} I_{Lk}(\mathbf{W}(\mathbf{x};\mathbf{p}_k)) \approx I(\mathbf{x}) \otimes N(0,\sigma^2), \qquad (1)$$

where $I_{Lk}(\mathbf{W}(\mathbf{x};\mathbf{p}_k))$ denotes the observed k-th frame in total N frames with the local motion of $\mathbf{W}(\mathbf{x};\mathbf{p}_k)$. Therein, $I(\mathbf{x})$ represents the real object appearance. In addition, $\otimes$ and $N(0,\sigma^2)$ respectively denote the convolution function and a Gaussian kernel of mean zero and standard deviation of σ.

Figure 3(b) shows the averaged image obtained from the sequence shown in Fig. 1; Fig. 3(a) shows a magnified observed image. The averaging operation uses 400 frames after the global motion removal. The operation eliminates the local motion, but the details in the observed frames are not visible in the averaged image.

(a) Observed image

(b) Averaged image

Figure 3. Frame averaging result.

3. Detail Recovery

This section describes the non-rigid deformation model with the B-spline basis function and the deformation parameter estimation method between two images. An objective function with a stabilization term is proposed for the parameter estimation method.

The B-spline basis function has the following advantages compared to the other basis functions: a smooth deformation of the image by a shift of a control point, a locality of the effect extent of a shift, affine transformation operability by movements of a set of control points, and a low computational complexity.

Furthermore, this section describes the multi-frame super-resolution reconstruction processing with the estimated non-rigid motion. The process recovers details lost in the averaging operation.

3.1. Non-Rigid Deformation Model

A displacement at an image position is obtainable from a weighted average of a set of displacement of control points located on the image using the B-spline basis function. We designate the vector $\mathbf{p} = [\,\Delta\hat{x}_1,\ \cdots\ ,\Delta\hat{x}_n,\ \Delta\hat{y}_1,\ \cdots\ ,\Delta\hat{y}_n\,]^\top$ as the deformation parameters, where the components of the vector are the horizontal and vertical displacement from the initial positions of n control points. The deformed position from original position $\mathbf{x} = (x,y)^\top$ is representable as follows when the initial positions are equally spaced [5]:

$$\mathbf{W}(\mathbf{x};\mathbf{p}) = \mathbf{x} + \mathbf{A}(\mathbf{x})\mathbf{p}. \qquad (2)$$

The $\mathbf{A}(\mathbf{x})$ denotes the following B-spline basis function matrix for the position $\mathbf{x}$.

$$\mathbf{A}(\mathbf{x}) = \begin{bmatrix} c_1 & \cdots & c_n & 0 & \cdots & 0 \\ 0 & \cdots & 0 & c_1 & \cdots & c_n \end{bmatrix}, \qquad (3)$$

In that equation, the B-spline basis c_i is representable as follows using the initial positions of the control points $\hat{\mathbf{x}}_{0i} = (\hat{x}_{0i}, \hat{y}_{0i})^\top$ and the interval between the control points (h_x, h_y).

$$\begin{aligned} c_i &= \beta\left(\frac{x - \hat{x}_{0i}}{h_x}\right)\beta\left(\frac{y - \hat{y}_{0i}}{h_y}\right) \qquad (4) \\ \beta(t) &= \begin{cases} 2/3 - (1 - |t|/2)t^2 & \text{, if } 0 \leq |t| \leq 1 \\ (2 - |t|)^3/6 & \text{, if } 1 < |t| < 2 \\ 0 & \text{, otherwise} \end{cases} \end{aligned}$$

The B-spline basis c_i can be computed in advance in this case, with the image size and the interval of the control points. Furthermore, almost all components in c_i become zero because of the locality of the effect extent of displacement of a control point. These enable a lower computational cost for image transformation than the other basis functions, including the TPS function.

Figure 4 illustrates a deformation caused by a shift of a control point. The white and red circles in the figure denote the control points. The shift of the centered red circle deforms the image, as illustrated in the right figure. The effect extent is limited in the green area.

3.2. Parameter Estimation using the Area-Based method

For the non-rigid motion parameter estimation, a *source image* S and a *target image* T respectively denote a reference image and an image to be deformed with the estimated motion parameter, in this article.

Figure 5 presents a diagram of the area-based parameter estimation method, which estimates the deformation parameter $\mathbf{p}$ by minimizing the error between the source image S and the target image T deformed with the parameter $\mathbf{p}$. However, the parameter $\mathbf{p}$ becomes unstable for a region with little texture because the error differs little as $\mathbf{p}$ changes.

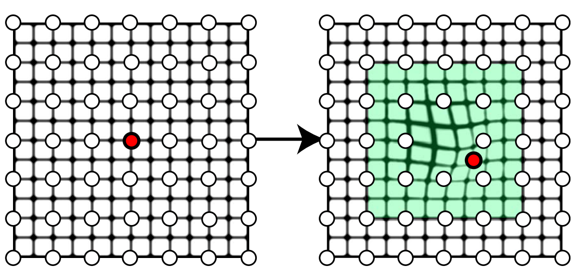

Figure 4. Shift of a control point and its influential area.

The proposed objective function $E(\mathbf{p})$ to be minimized includes the stabilization term (the second term), as

$$\begin{aligned} E(\mathbf{p}) &= \sum_{\mathbf{x}} |T(\mathbf{W}(\mathbf{x};\mathbf{p})) - S(\mathbf{x})|^2 \\ &\quad + \gamma \sum_{\mathbf{x}} \left\| \lambda(\mathbf{x})^{-1}\mathbf{A}(\mathbf{x})\mathbf{p} \right\|^2, \qquad (5) \\ \lambda(\mathbf{x}) &= \mathrm{diag}\left[\frac{\partial T(\mathbf{W}(\mathbf{x};\mathbf{p}))}{\partial \mathbf{W}}\right], \end{aligned}$$

where $\lambda(\mathbf{x})$ denotes a diagonal matrix that has image gradients at the point of interest in its diagonal components. The γ denotes a weight for the stabilization term, which can be determined empirically considering the image contrast. Too small a weight of γ renders the estimated parameter unstable; too large a weight makes the parameter stay at its initial value.

The stabilization term is a product of the inverse of the image gradient and the displacement of pixels. The term has less effect at a region having a large image gradient: the deformation parameter $\mathbf{p}$ can be large if the region has a rich texture. On the other hand, the stabilization term has a considerable effect for a region having a small gradient: the parameter remains at its initial value if the region has less texture. The stabilization term enables accurate deformation parameter estimation with stability of results.

Gauss-Newton method is used to minimize the objective function $E(\mathbf{p})$. The update of the deformation parameter is derived as

$$\begin{aligned} \mathbf{p}_{l+1} &= \mathbf{p}_l + \Delta\mathbf{p} = \mathbf{p}_l - \mathbf{H}^{-1}\mathbf{b}, \qquad (6) \\ \mathbf{H} &= \sum_{\mathbf{x}} \mathbf{g}(\mathbf{x})\mathbf{g}(\mathbf{x})^\top, \\ &\quad + \gamma \sum_{\mathbf{x}} \left(\lambda(\mathbf{x})^{-1}\mathbf{A}(\mathbf{x})\right)^\top \lambda(\mathbf{x})^{-1}\mathbf{A}(\mathbf{x}), \\ \mathbf{b} &= \sum_{\mathbf{x}} \mathbf{g}(\mathbf{x})\Delta I(\mathbf{x}), \\ \mathbf{g}(\mathbf{x})^\top &= \frac{\partial T(\mathbf{W}(\mathbf{x};\mathbf{p}_l))}{\partial \mathbf{W}}\mathbf{A}(\mathbf{x}), \\ \Delta I(\mathbf{x}) &= T(\mathbf{W}(\mathbf{x};\mathbf{p}_l)) - S(\mathbf{x}), \end{aligned}$$

where l represents an iteration number.

3.3. Super-Resolution Image Reconstruction

An image sequence that is influenced by optical turbulence includes many samples at different positions of the object as the local motion, even if the sequence is captured by a stationary camera for a static object. The local motion allows reconstruction of a higher resolution image from several low-resolution observations. In this section, the multi-frame super-resolution reconstruction [3],[4] is explained briefly, but the motion in

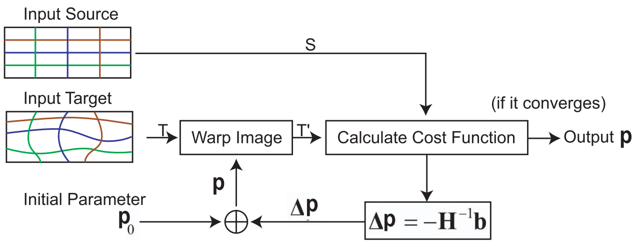

Figure 5. Area-based deformation parameter estimation.

the observed image differs from the well-known processing.

The super-resolution image reconstruction models the camera observation of a higher resolution or continuous image, as illustrated in Fig. 6. The observation is a low-resolution digital image with estimated motion. The higher resolution image to be estimated is updated by the error between the real observations and the simulated observations generated from the camera model. This process is equivalent to minimizing the following objective function using an optimization method such as conjugate gradient method.

$$f(\mathbf{z}) = \sum_{k=1}^{M} \|I_k - \mathbf{DFB}_k\mathbf{z}\|^2 + \alpha \|\mathbf{Lz}\|^2 , \qquad (7)$$

In the equation, $\mathbf{z}$ and $\mathbf{B}_k$ respectively denote the high-resolution image and the deformation matrix; $\mathbf{F}$ and $\mathbf{D}$ respectively represent a camera imaging model including the point spread function of the optics and a down sampling matrix from the high-resolution image to the low-resolution observation. Also, I_k and M respectively denote the k-th low-resolution observed image and the total number of the low-resolution images. In addition, $\mathbf{L}$ and α respectively denote a high-frequency component detection filter matrix and a weight parameter. Too small a weight of α renders the reconstruction unstable (noisy), whereas too large a weight creates a blurred image. Through some trials, an adequate value can be found to reconstruct the image.

The averaged image described in Section **2.2.** is used as the initial high-resolution image to minimize the objective function in Eq. (7).

The local motion of the k-th frame is used for the deformation matrix $\mathbf{B}_k$ in Eq. (7). The local motion is estimated as follows. First, the averaged image is generated from the sequence after compensating the global motion. Second, the local motion is estimated for the k-th frame. The averaged image is set as the target image T; the convolution of a Gaussian kernel and the k-th frame after compensating the global motion is set as the source image S.

The unknown high-resolution image $\mathbf{z}$ has no deformation but the observations have local motions. The

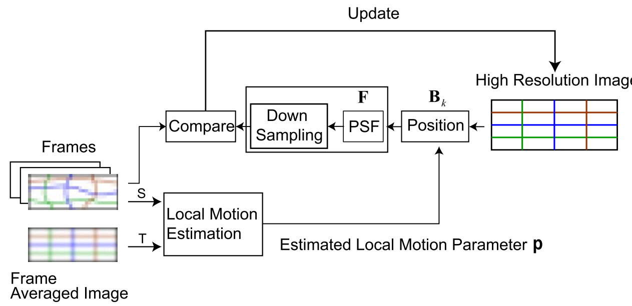

Figure 6. Super-resolution image reconstruction for detail recovery.

local motion for the super-resolution is the motion to deform the high-resolution image to correspond to the low-resolution observations. The input frames are used for the source images S, the averaged image is used for the target image T, as shown in Fig. 6.

The reason for using the Gaussian convolution is that the averaged image has a blur compared to the input frame. The standard deviation of the Gaussian kernel is obtainable from the motion distribution of the sequence, as shown in Fig. 2, and a Gaussian fitting over the histogram of the distribution. However, in real situations, the parameter estimation method described in **3.2.** performs for two images that have slightly different blur kernels. In our experiments, the standard deviation of the Gaussian kernel is determined empirically as the smallest value with stability and detailed deformation outputs between 1.5 and 0.8.

The real object appearance can also be estimated as averages of the optical flows obtained from the sequence [10]. However, optical flow estimation requires features or textures in an image; a corresponding position for a textureless region must be obtained through an interpolation from neighboring flows. Furthermore, the estimated optical flow includes some error because the image patch pair that is used to estimate the optical flow is deformed. The method described in **3.2.** directly and automatically estimates the image deformation whether the image has a sufficient texture or not.

4. Experimental Results

We conducted experiments using both synthetic images and real sequences.

The size of all synthetic images is 60×60 [pixels] to reduce the computational time. The control points of 9×9 are placed at even intervals on the image. The synthetic image is deformed with B-spline function by giving displacements to the control points at random (rectangular distribution with maximum 3 pixels). The displacement of the non-rigid deformation with the B-spline basis function is less than the shift values of the control points; the deformation in the synthetic images is less than 3 pixels. Additionally, all synthetic images have additive Gaussian noise for the pixel values with standard deviation of 5.0.

The real sequences were captured using a 3-CCD digital videocassette camera (DCR-VX2000; Sony Corp.) in the progressive scan mode (15 frames/second). The image size is 720×480 [pixels].

4.1. Local Motion Estimation Accuracy

Figures 7(a) and 7(b) respectively depict the synthetic images with and without deformation for the first experiment.

Figure 8 presents the results of estimation accuracy. A deformed image from (a) by the estimated motion parameters is compared with the image (b) in positional root-mean-square error (RMSE) [pixel]. The horizontal and vertical axes respectively denote the square root of the number of control points and the positional RMSE. The dashed line denotes the RMSE between the images shown in Fig. 7(a) and 7(b), that is, the RMSE without the local motion estimation. The solid line represents the RMSE between the deformed image by the estimated parameters and the image (b). The RMSE is always less than that in the case without local motion estimation. The RMSE takes a minimum value at the 9×9 control points, which is the same as the number for the synthetic deformed image (b). The fewer control points cannot express the exact deformation, although the noise and texture slightly affect the results with many control points.

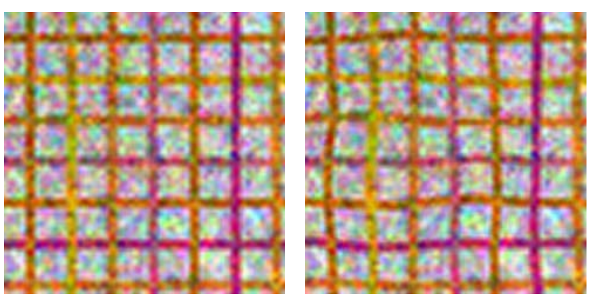

(a) Without deformation (b) With deformation

Figure 7. Synthetic images used for testing motion estimation accuracy.

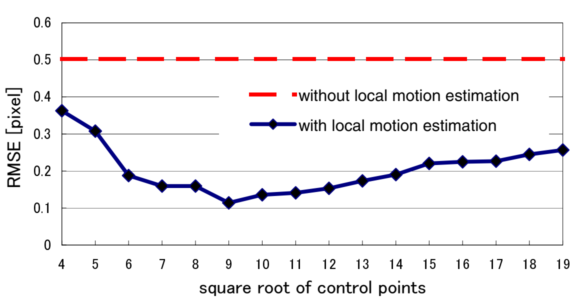

Figure 8. RMSE of position using estimated local motion with respect to density of control points.

4.2. Local Motion Estimation Stability

Figure 9(a) and 9(b) respectively portray synthetic images with and without deformation for the second experiment. The synthetic images have textureless regions compared to images for the first experiment. The local motion of image (b) is estimated for the source image (a), with 9×9 control points.

Figure 10(a) shows many initial positions in the image shown in Fig. 9(b). The initial positions do not correspond to the control points; they represent many positions of pixels in the image. Figures 10(b) and 10(c) respectively show the motion estimation results (corresponding pixel positions) without ($\gamma = 0$ in Eq. (5)) and with ($\gamma = 5.0$), the stabilization term. The image intensity is reduced in Fig. 10 for better visibility. The local motion estimation in Fig. 10(b) fails in the region with less texture, although the results are stable for all regions in Fig. 10(c), underscoring the effectiveness of the stabilization term in the proposed parameter estimation method.

Figure 11 presents the differing intensities RMSE for the whole image between a deformed image using the estimated local motion parameters and the image (b). The triangle marks represent the results without the stabilization term, which result in instability with

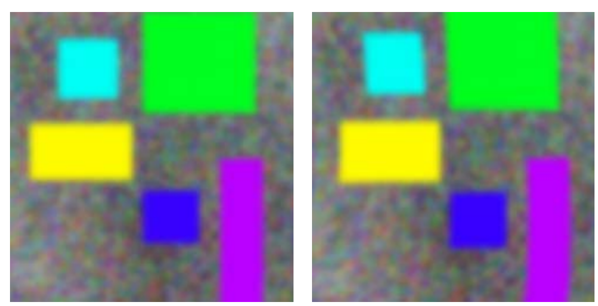

(a) Without deformation (b) With deformation

Figure 9. Synthetic images used for testing motion estimation stability.

(a) initial positions (b) Without stab. term (c) With stab. term

Figure 10. Motion estimation results with and without the stabilization term.

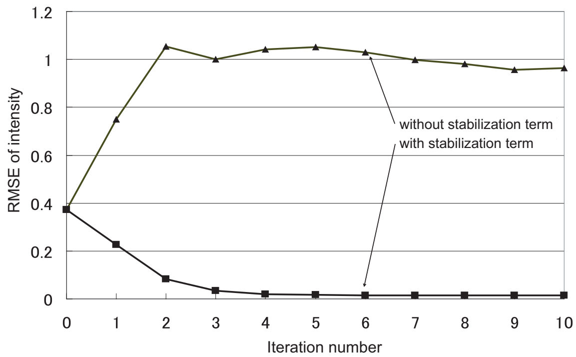

Figure 11. RMSE of intensity with respect to the iteration number.

(a) Observed image

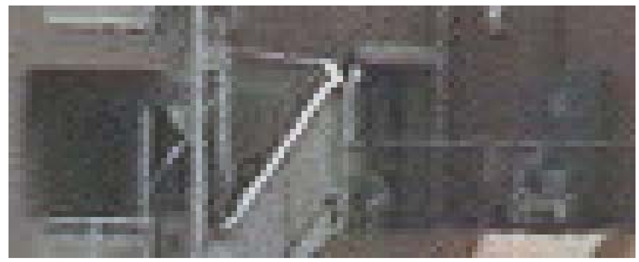

(b) Magnified observed image

(c) Super-resolution result

Figure 12. Super-resolution result from sequential images that include optical turbulence for distant objects.

iteration. The square marks show the results with the stabilization term, showing the stability with iteration.

4.3. Super-Resolution Results

Figures 12 and 13 show the super-resolution reconstruction results from sequences under the influence of the optical turbulence. The image magnification ratio for the super-resolution is 4×4. Figures 12(a) and 13(a) portray the observed image; the white rectangle regions are processed. Figures 12(b) and 13(b) depict the magnified observations. Figures 12(c) and 13(c) show the super-resolution results.

The processed area is 110×40 [pixels] in Fig. 12(a). The local motion is estimated for this region with 14×7 control points. The averaged image is generated using 230 frames in the sequence. The local motion estimation and the super-resolution reconstruction are processed using the first 120 frames in the sequence. The resultant higher resolution image has less noise and contains more detailed information than the observations.

The processed area is 128×72 [pixels] in Fig. 13(a). The local motion is estimated for this region with 16×10 control points. The averaged image is generated using 400 frames in the sequence. The local motion estimation and the super-resolution reconstruction are processed using the same 400 frames in the sequence. The resultant higher resolution image also has less noise and more detailed information than the observations; for example, the door handle in the silver car is clearly distinguishable.

We have compared the results with enlarged original video frames by image interpolation such as Lanczos filter to confirm that our results are far beyond them.

The affine global motion is estimated for each frame in the sequence for the first frame as the reference in both reconstruction processes. The frame averaging operation uses images after compensating the estimated global motions. The local motion is estimated for each region in the frame for the frame-averaged image as the reference. To enhance the image resolution, the deformation for each frame is used as a different observation position for the super-resolution reconstruction process.

The computational time to estimate the global motion is negligible, although the local motion estimation takes much time. The use of more frames is better for generating the averaged image; all frames in the sequence are used for the averaging operation.

On the other hand, it takes around 30 seconds (Pentium4 2.8 GHz) to estimate the local motion for one frame in the white rectangle region shown in Fig. 12(a). The minimum number of frames is determined empirically for an effective super-resolution processing.

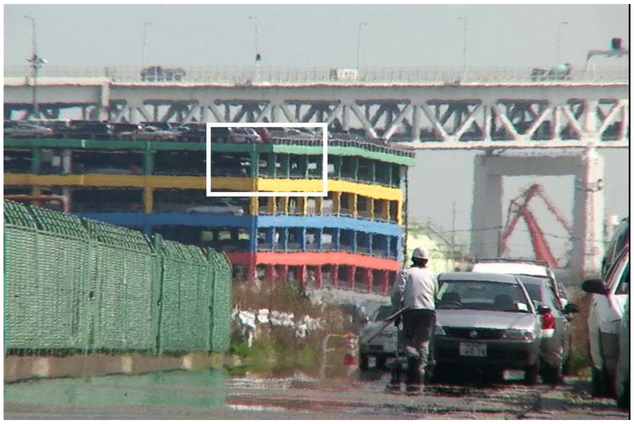

(a) Observed image

(b) Magnified observed image

(c) Super-resolution result

Figure 13. Super-resolution results from sequential images that include optical turbulence for distant objects.

5. Conclusions

This study has proposed an objective function for an area-based non-rigid registration technique dealing with textureless regions. The super-resolution reconstruction process was described using the non-rigid registration technique. After investigating characteristics of the non-rigid movement in the sequence under influence of the optical turbulence, an estimation method of the real object appearance was described. The super-resolution reconstruction is used to recover detailed information that is lost through estimation.

The number of control points was determined empirically; an automatic determination method remains as a future research theme. An exact model of the optical turbulence must be developed to determine the number of control points and the minimum number of frames for frame averaging. This development is another future research theme.

References

[1] A. Bartoli, E. V. Tunzelmann and A. Zisserman, "Augmenting Images of Non-Rigid Scene Using Point and Curve Correspondences," CVPR, vol. 1, pp. 699–706, 2004.

[2] F. L. Bookstein, "Principal Warps: Thin-Plate Splines and the Decomposition of Deformation," IEEE Trans. on PAMI, vol. 11, no. 6, pp. 567–585, 1989.

[3] T. Goto and M. Okutomi, "Direct Super-Resolution and Registration using Raw CFA Images," CVPR, vol. 2, pp. 600–607, 2004.

[4] R. C. Hardie, K. J. Barnard, and E. E. Armstrong, "Joint MAP Registration and High-Resolution Image Estimation using a Sequence of Undersampled Images," IEEE Trans. on IP, vol. 6, no. 12, pp. 1621–1633, 1997.

[5] J. Kybic and M. Unser, "Unwarping of Unidirectionally Distorted EPI Images," IEEE Trans. on Medical Imaging, vol. 19, no. 2, pp. 80–93, 2000.

[6] J. Kybic and M. Unser, "Fast Parametric Elastic Image Registration," IEEE Trans. on IP, vol. 12, no. 11, pp. 1427–1442, 2003.

[7] S. Lee, G. Wolberg and S. Y. Shin, "Scattered Data Interpolation with Multilevel B-Splines," IEEE Trans. on Visualization and Computer Graphics, vol. 3, no. 3, pp. 228–244, 1997.

[8] J. Lim and M.-H. Yang, "A Direct Method for Modeling Non-Rigid Motion with Thin Plate Spline," CVPR, vol. 1, pp. 1196–1202, 2005.

[9] D. Loeckx, F. Maes, D. Vandermeulen, and P. Suetens, "Non-Rigid Image Registration using a Statistical Spline Deformation Model," Proc. on Information Processing in Medical Imaging, pp. 463–474, 2003.

[10] H. Murase, "Surface Shape Reconstruction of a Non-Rigid Transparent Object using Refraction and Motion," IEEE Trans. on PAMI, vol. 14, no. 10, pp. 1045–1052, 1992.

[11] S. G. Narasimhan and S. K. Nayar, "Vision and the Atmosphere," IJCV, vol. 48, no. 3, pp. 233–254, 2002.

[12] R. Szeliski and J. Coughlan, "Spline-Based Image Registration," IJCV, vol. 22, no. 3, pp. 199–218, 1997.

[13] Z. Xie and G. E. Farin, "Image Registration using Hierarchical B-Splines," IEEE Trans. on Visualization and Computer Graphics, vol. 10, no. 1, pp. 85–94, 2004.